

Simulating streamer discharges in 3D with the parallel adaptive Afivo framework

Jannis Teunissen¹  and Ute Ebert^{2,3} 

¹ Department of Mathematics, Centre for mathematical Plasma Astrophysics, KU Leuven, Celestijnenlaan 200B, B-3001 Leuven, Belgium

² Centrum Wiskunde & Informatica (CWI), PO Box 94079, 1090 GB Amsterdam, Netherlands

³ Department of Applied Physics, Eindhoven University of Technology, PO Box 513, 5600 MB Eindhoven, The Netherlands

E-mail: jannis@teunissen.net

Received 21 July 2017, revised 21 September 2017

Accepted for publication 28 September 2017

Published 30 October 2017



CrossMark

Abstract

We present an open-source plasma fluid code for 2D, cylindrical and 3D simulations of streamer discharges. The code is based on the Afivo framework, which features adaptive mesh refinement on quadtree/octree grids, geometric multigrid methods for Poisson's equation, and OpenMP parallelism. We describe the numerical implementation of a fluid model of the drift-diffusion-reaction type, combined with the local field approximation. Then we demonstrate its functionality with 3D simulations of long positive streamers in nitrogen in undervolted gaps. Three examples are presented. The first one shows how a stochastic background density affects streamer propagation and branching. The second one focuses on the interaction of a streamer with preionized regions, and the third one investigates the interaction between two streamers. The simulations use up to 10^8 grid cells and run in less than a day; without mesh refinement they would require more than 10^{12} grid cells.

Keywords: streamer discharge, 3D simulation, adaptive mesh refinement, streamer interaction, streamer branching, plasma fluid model, geometric multigrid

(Some figures may appear in colour only in the online journal)

1. Introduction

Streamer discharges [1–3] are a generic stage of electric breakdown of nonconducting matter, dominated by strong space charge effects at the tips of growing discharge channels. They occur as precursors of sparks, arcs, and lightning leaders, both in nature and in high voltage and plasma technology. Streamers are directly visible as so-called sprites in the mesosphere [4], and they are used in applications such as surface processing [5], sterilization and disinfection [6] or wound healing [7], often in the form of atmospheric pressure plasma jets [8].

Streamers grow due to strong field enhancement at the tips of their elongated partially ionized channels. The high local fields support the local growth of ionization due to electron impact ionization. Simulating this process has proven to be challenging for a number of reasons:

- Problems such as streamer branching or the interaction between streamers require a three-dimensional description, as illustrated in figure 1.

- A fine grid spacing is required to accurately resolve the thin charge layers around streamer heads that create the local field enhancement, see figure 2. Due to the strongly non-linear growth of streamers, it is usually not possible to obtain an approximate solution on a coarse grid.
- Time-dependent simulations are required. Due to the high electric field at streamer tips, where the mesh spacing is small, small time steps have to be used.
- At each time step, Poisson's equation has to be solved to obtain the electrostatic potential and field. The non-local nature of this equation complicates the parallelization of streamer models.

The physics of streamer discharges is mostly governed by electrons, because ions gain energy more slowly and lose it more easily in collisions. Both plasma fluid models and kinetic/particle-in-cell models have been used to simulate streamers. In fluid models particle densities (and sometimes also momentum or energy densities) evolve in time, using pre-calculated transport coefficients as input data. In kinetic

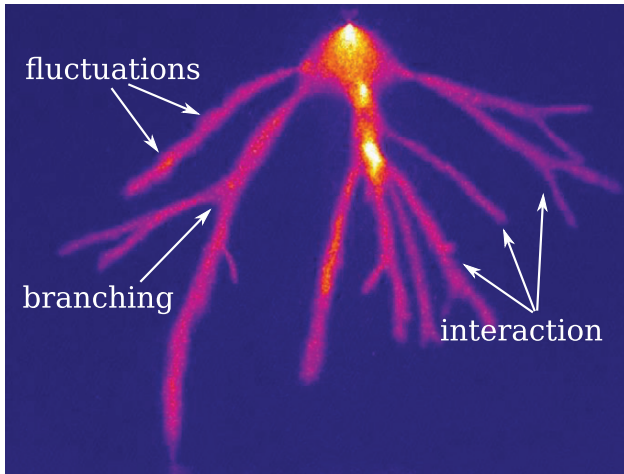


Figure 1. Experimental picture of positive streamers, showing why 3D simulations are often required: streamers branch and interact, and single streamers often show fluctuations which cannot be captured with axisymmetric models. Reproduced from [9]. © IOP Publishing Ltd. All rights reserved (air at 293 K and 0.4 bar, 16 kV applied to a 4 cm gap).

simulations, the electron distribution function $f(\vec{x}, \vec{v}, t)$ evolves in time, using cross sections as input data. Kinetic simulations typically require a large number of particles and smaller time steps than fluid simulations, so that their computational cost is considerably higher.

The history of streamer modeling goes back several decades; early work includes for example [1, 10]. Most models developed since have been of the plasma fluid type, and such models typically face (at least) two challenges: solving the fluid equations with high accuracy but without introducing unphysical oscillations, and efficiently computing the electric field at each iteration. For discharges in air, an additional challenge has been computation of the photoionization source term, see for example [11, 12].

Different numerical methods have been used to solve the fluid equations, for example the Scharfetter–Gummel scheme in [12, 13], the flux-corrected transport method in [14, 15], the use of flux/slope limiters in [16–18] and the use of a WENO scheme in [19]. Finite volume methods have been popular because they can relatively easily be implemented on structured grids, because they are conservative by construction, and because efficient methods are available for advection problems. To adapt models to more complex discharge geometries the finite element method has also been used, for example in [20–22].

We now briefly review the development of three-dimensional simulations. The first demonstration of a 3D fluid simulation was given in [23]. In [24], parallel fluid simulations with adaptive mesh refinement (AMR) were performed using Paramesh, but the main bottleneck was the Poisson solver. Later work includes a 2.5D fluid model with AMR, parallelized over axial modes [25]. Kinetic [26, 27] and hybrid kinetic/fluid [28] 3D models without AMR have also been employed, and more recently kinetic models with AMR have been used [29, 30]. Other work includes 3D simulations with a finite element code [31] and a proof-of-concept of 3D simulations in

transformer oil with OpenFoam [32]. A notable development was the 3D fluid model with AMR presented in [33], which is commercially available. The adaptation of parallel multigrid methods from the Gerris flow solver [34] made it possible to perform relatively large scale 3D simulations.

Here, we present Afivo⁴-streamer, an open-source fluid model for the simulation of streamer discharges. Both 2D, axisymmetric and 3D simulations are supported, but the focus here is on 3D, which is computationally most challenging. Afivo-streamer is based on the Afivo framework [35], which provides quadtree/octree adaptive mesh refinement, a geometric multigrid solver, shared-memory parallelism, and routines for writing output. The first successful application of Afivo-streamer can be found in [36]. The main contribution of Afivo-streamer is that it provides efficient and open-source computational infrastructure for 2D, 3D and axisymmetric streamer simulations.

The paper is organized in two parts. In the first part (section 2), the numerical implementation of Afivo-streamer is described. In the second part (section 3), we demonstrate the code’s functionality with three 3D examples.

2. Model description

The implementation of the different components of Afivo-streamer is described below. The source code is available online through [37] under an open source (GPLv3) license.

2.1. Afivo AMR framework

Adaptive mesh refinement is essential for 3D streamer simulations. Without AMR, the fine grid spacing that is required near the streamer head severely restricts the size of the computational domain. Here, the open-source Afivo framework [35] is used to provide AMR and parallelization for streamer simulations. The functionality of Afivo is summarized below; for more details we refer to [35].

2.1.1. Adaptive quadtree/octree grids. Afivo supports quadtree (2D) and octree (3D) grids. A quadtree/octree grid consists of blocks of N^D cells, where N is an even number (here we use $N = 8$) and D is the problem dimension. One or more of these blocks defines the coarse grid. A coarse grid block can be refined by covering it with 2^D child blocks, which each have half the grid spacing. This process can be repeated recursively, leading to an adaptively refined mesh that still has a quite regular structure, as illustrated in figure 3.

Afivo provides routines for adapting the mesh, but does not come with built-in refinement criteria. The criteria used here are discussed in section 2.5. Afivo does ensure *proper nesting*, which means that neighboring boxes differ by at most one refinement level. Different methods for interpolating from coarse to fine grids are included. For restriction (going from fine to coarse grids) simple averaging is implemented, in which a coarse cell gets the average value of the four (2D) or eight (3D) fine cells that cover it.

⁴ Afivo stands for ‘adaptive finite volume octree’.

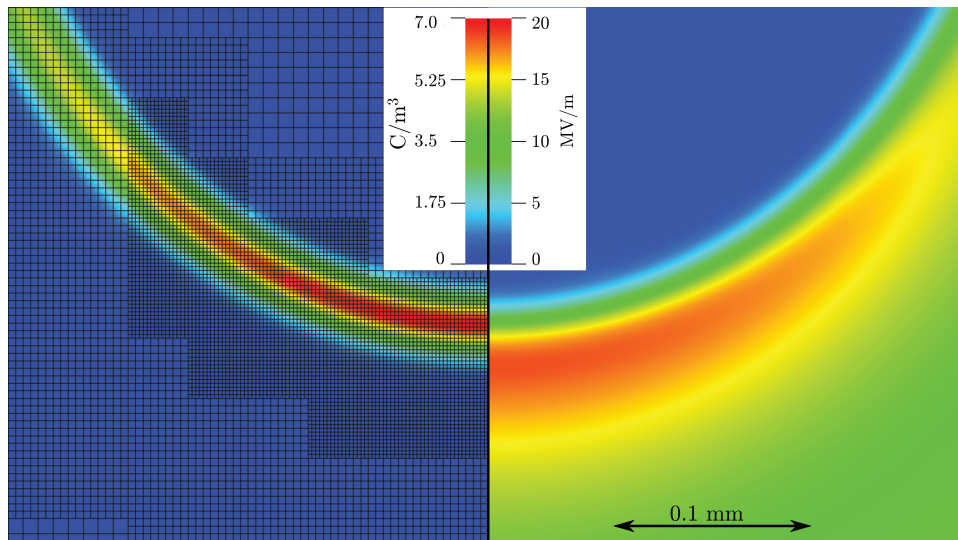


Figure 2. Cross section through a streamer head, showing the charge density (left) and electric field strength (right). The numerical mesh was generated according to the criteria described in section 2.5, using equation (9) with $c_0 = 1.0$ and $c_1 = 1.2$.

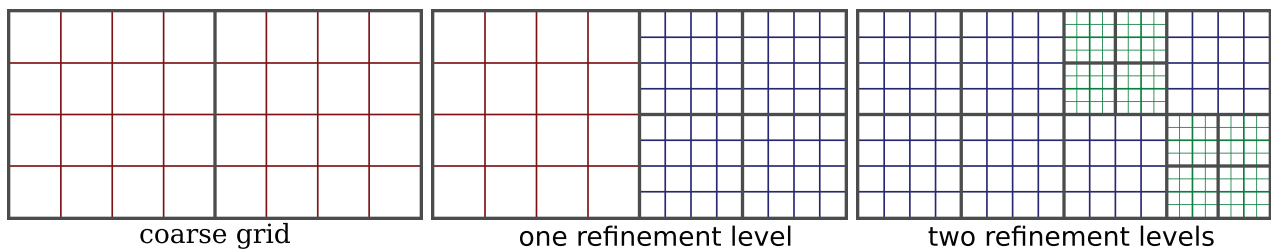


Figure 3. Left: example of a quadtree grid consisting of two blocks of 4×4 cells. The middle and right figure show how the mesh can be refined by recursively adding new blocks, each having half the grid spacing of their parent.

Afivo provides storage for cell-centered and face-centered variables. For the cell-centered variables, each grid block contains storage for one layer of so-called ghost cells. How these ghost cells are filled depends on whether there is a physical boundary, a refinement boundary or a ‘normal’ boundary between blocks of the same refinement level. The use of ghost cells simplifies the implementation of numerical schemes, and also helps in performing parallel computations.

2.1.2. Geometric multigrid solver. One of the key computational challenges in streamer simulations is quickly solving Poisson’s equation

$$\nabla \cdot (\varepsilon \nabla \phi) = -\rho, \quad (1)$$

to obtain the electrostatic potential ϕ from the charge density ρ , where ε is the dielectric permittivity. The electrostatic field can then be determined as $\vec{E} = -\nabla \phi$. Poisson’s equation has to be solved at every time step and with high spatial resolution within the ionization fronts, and its non-local nature prevents a straightforward parallel solution. Therefore, the Poisson solver is often the most time-consuming part of streamer simulations. Afivo implements geometric multigrid routines [38, 39], which are among the fastest methods for solving elliptic equations such as (1).

Multigrid methods are iterative solvers which cycle over a hierarchy of grids. Short-wavelength errors are efficiently reduced on fine grids, and long-wavelength errors on coarse

grids, by using an appropriate smoothing procedure. There are many varieties of multigrid, which differ in for example their multigrid cycle, smoothing procedure, grid hierarchy or interpolation method. For a detailed description of multigrid methods, which we cannot give here, we refer to e.g. [38–40].

Afivo supports a V-cycle and an FMG (full multigrid) cycle, both using a cell-centered discretization for the solution ϕ and the right-hand side ρ . An FMG cycle is more expensive than a V-cycle, but it typically gives a solution within the discretization error in one or two iterations. Both cycles are implemented using the full approximation scheme, which means that the computed solution is available at all grid levels (in some multigrid methods, only the correction to the solution is computed on coarse grids). Afivo includes Gauss–Seidel red-black smoothers that can be used for constant ε problems, and to some extent also for problems where ε varies, see [35]. It is currently not possible to include internal boundary conditions, for example to define a curved electrode, although work in that direction is ongoing.

Afivo’s multigrid can handle adaptively refined quadtree/octrees. Near refinement boundaries, fine-grid ghost cells are filled in a ‘conservative’ way, to obtain a consistent solution on all grid levels. The procedure can be illustrated using figure 4, which shows a refinement boundary in a quadtree mesh. If we solve equation (1) (with constant ε) on this grid, then we should have

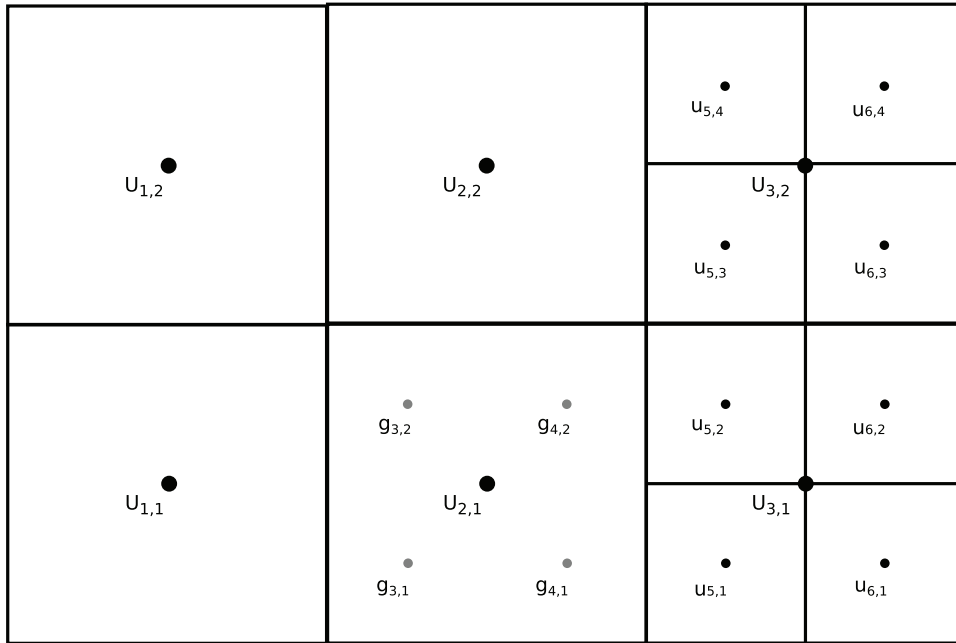


Figure 4. Figure to help explain how equations are discretized near a refinement boundary in a quadtree. The dots indicate cell centers, with coarse grid values are indicated by U_{ij} , fine grid values by u_{ij} and ghost cells by g_{ij} . Not all ghost cells are indicated. A coarse cell with index (i, j) is covered by fine cells with indices $(2i - 1, 2j - 1)$ up to $(2i, 2j)$.

$$(U_{3,1} - U_{2,1})/H = \frac{1}{2} [(u_{5,1} - g_{4,1})/h + (u_{5,2} - g_{4,2})/h]. \quad (2)$$

The left-hand side of this equation corresponds to the coarse flux $\partial_x U$ over the bottom half of the refinement boundary, and the right-hand side to the average fine flux. To see why these fluxes should match, it can be helpful to think of equation (1) as a steady-state diffusion problem. With Afivo’s standard restriction method $U_{3,1} = (u_{5,1} + u_{5,2} + u_{6,1} + u_{6,2})/4$, several conservative ghost cells schemes can be constructed, for example:

$$g_{4,1} = \frac{1}{2}U_{2,1} + u_{5,1} - \frac{1}{4}(u_{5,2} + u_{6,1}),$$

$$g_{4,2} = \frac{1}{2}U_{2,1} + u_{5,2} - \frac{1}{4}(u_{5,1} + u_{6,2}).$$

More details on the ghost cell procedure and the extension to the 3D case can be found in [35].

In the Afivo-streamer code, an FMG cycle is used to compute the electric potential at the start of a simulation. For each subsequent update of the potential a number of V-cycles is used (here two), which take the previous solution as an initial guess. This exploits the fact that there are only small changes in the potential between time steps.

In streamer simulations with AMR, the fine grid ideally covers a relatively small region. As discharges propagate, the mesh has to follow their features, meaning it changes frequently in time. A key advantage of *geometric* multigrid methods is that they require almost no extra computation when the mesh changes, in contrast to matrix-based (direct) methods.

2.1.3. Parallelization. Afivo incorporates shared-memory parallelization using OpenMP, which means that it can use

one up to e.g. 32 cores, depending on the available hardware. Since the quadtree/octree grid is naturally divided into blocks, the parallelization is performed over these blocks. This is implemented with OpenMP constructs around all the relevant loops in the framework. Afivo also provides parallel loop methods, which given a routine for a single block will apply that routine on all blocks in parallel. In cases where more flexibility is required, users can also write their own parallel loops over the quadtree/octree blocks.

The scaling of codes based on Afivo is typically limited by the memory bandwidth of the computer: when relatively ‘cheap’ algorithms are used, transferring data from memory to each CPU core and back takes most of the time. For the multigrid methods, a further challenge is that coarse grid levels contain few data points, hampering their parallel efficiency, see e.g. [39]. An example of the scaling behavior is given in section 3.2, which shows a maximal speedup of about a factor 7 using 28 CPUs. However, since we have not yet tried to optimize the parallel efficiency of Afivo-streamer, better scaling is probably possible in the future.

2.1.4. Writing output. When doing 3D simulations with AMR, writing and visualizing output can be challenging. Afivo comes with support for writing VTK unstructured files and Silo files, which can be visualized with e.g. Visit [41]. For 3D simulations, the Silo format is more efficient, as it groups grid blocks into larger rectangular regions. The Silo files also include ghost cell information, which helps to ensure smooth visualizations near refinement boundaries. For a 3D streamer simulation output can get pretty large: using for example five variables and 2×10^7 grid cells, a single file is about a gigabyte.

2.2. Fluid model equations

The fluid model used here is of the drift-diffusion-reaction type with the local field approximation [42]. It keeps track of the electron density n_e and the positive ion density n_i :

$$\partial_t n_e = \nabla \cdot (\mu_e n_e \vec{E} + D_e \nabla n_e) + \bar{\alpha} \mu_e E n_e, \quad (3)$$

$$\partial_t n_i = \bar{\alpha} \mu_e E n_e. \quad (4)$$

Here, $\bar{\alpha}$ is the effective ionization coefficient, μ_e the electron mobility, D_e the electron diffusion coefficient and \vec{E} the electric field. With the *local field approximation* μ_e , D_e and $\bar{\alpha}$ are functions of the local electric field strength. These coefficients can be computed with a Boltzmann solver [43, 44] or particle swarms [45], or they can be measured experimentally. The fluid equations are coupled to the electrostatic field, which is computed as

$$\vec{E} = -\nabla \phi, \quad (5)$$

$$\nabla^2 \phi = -e(n_i - n_e)/\epsilon_0 \quad (6)$$

where ϕ is the electric potential, ϵ_0 the permittivity of vacuum and e the elementary charge. The electric potential is computed with the multigrid routines from Afivo, described in section 2.1.

Different types of plasma fluid models can be implemented in Afivo-streamer. More advanced models could for example include an equation for the momentum and/or energy density, and let the transport coefficients depend on the mean electron energy, see e.g. [46, 47]. The mean energy is then given by Q/n_e , where Q is the energy density. Such models capture more of the physics, as demonstrated in e.g. [48]. However, the ratio is Q/n_e hard to define when $n_e \rightarrow 0$, making such models less robust than the one used here. Furthermore, a hyperbolic system with multiple coupled equations is generally harder to solve than a scalar one.

For electric discharges in air, photoionization is often an important process [49]. Excited nitrogen molecules can emit UV photons which are able to ionize oxygen molecules. Such a non-local source of free electrons is particularly important for positive streamers, which require free electrons ahead of them to grow. Afivo-streamer contains a Monte Carlo procedure for photoionization, which can take into account stochastic fluctuations due the finite number of photons. The procedure is described in chapter 11 of [50], and in a forthcoming paper we will investigate the effect of stochastic photoionization on streamer branching. In the present paper, we focus on discharges in pure nitrogen without photoionization, using a background density of electrons and positive ions.

2.3. Spatial discretization

We use an explicit finite volume approach, in which the following quantities are defined at cell centers: the electron/ion density, the electric potential, and the electric field strength. The electron fluxes and the electric field components are defined at cell faces. The spatial discretizations used in Afivo-streamer are generally second order accurate. However, near

extrema and shocks the flux-limited scheme reduces to first order, and the same happens near refinement boundaries due to the use of linear interpolation.

Afivo's multigrid routines compute the electric potential from the charge density, as discussed in section 2.1.2. From the cell-centered electric potential ϕ , the electric field at cell faces is computed by central differencing, so that the x -component is computed as

$$E_x^{i+1/2,j,k} = (\phi^{i,j,k} - \phi^{i+1,j,k})/\Delta x.$$

The electric field strength at cell centers is then computed as $E^{i,j,k} = \sqrt{E_x^2 + E_y^2 + E_z^2}$ where $E_x = (E_x^{i-1/2,j,k} + E_x^{i+1/2,j,k})/2$ is the average x -component at the cell center, $E_y = (E_y^{i,j-1/2,k} + E_y^{i,j+1/2,k})/2$, and similarly for E_z .

We follow the approach from [16] for the discretization of the fluid equations. The advective part of the flux is computed using the Koren limiter [51]. The electron velocity at a cell face is then computed as

$$v_x^{i+1/2,j,k} = -\mu(E^*)E_x^{i+1/2,j,k},$$

where $E^* = (E^{i,j,k} + E^{i+1,j,k})/2$ is the electric field strength $|\vec{E}|$ at the cell face. For brevity, we now omit the extra indices j, k . If $v_x^{i+1/2} < 0$, the advective flux between cell i and $i+1$ is given by

$$f_x^{i+1/2} = v_x^{i+1/2} \left(n_e^{i+1} - \psi \left(\frac{n_e^{i+2} - n_e^{i+1}}{n_e^{i+1} - n_e^i} \right) (n_e^{i+1} - n_e^i) \right), \quad (7)$$

and if $v_x^{i+1/2} \geq 0$, it is given by

$$f_x^{i+1/2} = v_x^{i+1/2} \left(n_e^i + \psi \left(\frac{n_e^i - n_e^{i-1}}{n_e^{i+1} - n_e^i} \right) (n_e^{i+1} - n_e^i) \right), \quad (8)$$

where $\psi(x)$ is the Koren limiter, given by

$$\psi(x) = \max(0, \min(1, (2+x)/6, x)).$$

The y and z components are computed similarly. Note that the above equations, if directly implemented, could cause division by zero. Our numerical implementation avoids this; it is described in appendix B of [50]. The diffusive flux between cells i and $i+1$ is computed using central differences, and is given by

$$f_x^{i+1/2} = D_e(E^*)(n_e^i - n_e^{i+1})/\Delta x,$$

with E^* defined as above.

To implement the above discretization near the boundary of a block, we use ghost cells. Two ghost cells are required⁵, because the flux $f_x^{i+1/2}$ from equation (7) depends on n_e^{i+1} and n_e^{i+2} . These ghost cells are filled by linear interpolation. For a quadtree (in 2D), we use the following scheme for the first ghost cell, with indexes referring to those of figure 4:

$$g_{4,2} = \min[(3U_{2,1} + U_{2,2} + 2u_{5,2})/6, 2U_{2,1}].$$

This can for example be seen as first linearly interpolating between $U_{2,1}$ and $U_{2,2}$ to get $g_{4-1/2,2}$, and then linearly

⁵ Since blocks contain storage for only one layer of ghost cells, a temporary array is used to include a second layer of ghost cells.

interpolating between $g_{4-1/2,2}$ and $u_{5,2}$ to get $g_{4,2}$. We limit $g_{4,2}$ to at most $2U_{1,1}$ to ensure that $U_{1,1}$ stays positive when the electron flux goes from coarse to fine. The second ghost cell is filled using linear interpolation, using

$$g_{3,2} = (2U_{2,1} + U_{1,1} + U_{2,2})/4.$$

In 3D, the same interpolation approach is used, but the schemes then depend on three neighboring values. Because we use linear interpolation, the accuracy of our discretization drops to first order near refinement boundaries. If instead higher order interpolation was used that could lead to other problems, such as the generation of new extrema or negative values. Finally, we remark that at refinement boundaries the coarse fluxes are replaced by the average fine flux, to ensure mass conservation.

To efficiently look up transport coefficients we convert them to a *lookup table*. This table stores the coefficients at regularly spaced electric field strengths, linearly interpolating the input data, e.g. from BOLSIG+ [43]. To look up values for a given field strength, the corresponding index in the table is computed, after which linear interpolation is employed. By default, the table is constructed up to $E_{\max} = 35 \text{ MV m}^{-1}$ using 1000 steps.

2.4. Temporal discretization

Time stepping is performed as in [16], using the second order accurate explicit trapezoidal rule. This method is strong stability preserving (SSP) and has favorable properties when combined with the Koren limiter [52]. Our implementation advances over Δt as follows:

- (i) Store the original electron and ion densities.
- (ii) Compute fluxes and source terms, then perform a forward Euler step over Δt and compute a new electric field.
- (iii) Compute fluxes and source terms, then perform another forward Euler step over Δt .
- (iv) Average the new electron and ion densities (advanced over $2\Delta t$) with the stored initial ones. Then compute a new electric field at $t + \Delta t$ from the resulting charge density.

All the grids are advanced using the same global time step. We limit Δt according to several criteria. The first is a CFL condition

$$\Delta t \sum |v_i|/\Delta x < 0.5,$$

where v_i are the velocity components and Δx the grid spacing, which is equal in all directions. This condition is more strict than necessary for stability, but we found that a CFL number of 0.5 gives a good balance between accuracy and computational cost. To ensure stability for the combined advective and diffusive fluxes, we require

$$\Delta t \sum |v_i|/\Delta x + \Delta t (2DD_e)/\Delta x^2 < 1.0,$$

where D is the problem dimension and D_e the electron diffusion constant. Finally, the time step is also limited by the dielectric relaxation time

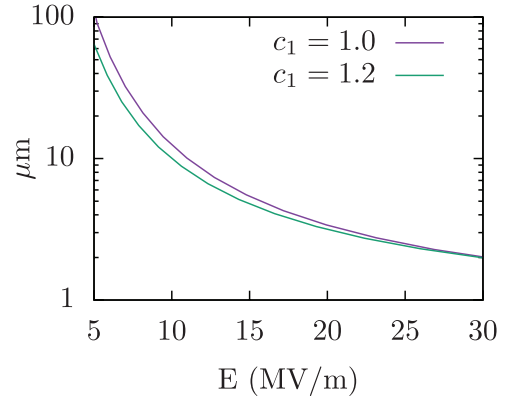


Figure 5. The refinement criterion of equation (9) for $c_1 = 1.0$ and $c_1 = 1.2$, with $c_0 = 1.0$ for both cases. With a larger value of c_1 , there is more refinement at low to intermediate electric fields. Data for nitrogen at 1 bar was used for $\alpha(E)$, as described in section 3.1.

$$\Delta t < \varepsilon_0/(e\mu_e n_e).$$

These requirements for Δt are evaluated at stage (iii) of our time stepping scheme, where the required quantities are already available. The next time step is then obtained by multiplying with a safety factor (default 0.9).

2.5. Refinement criterion

The growth of positive streamers is dominated by electron impact ionization. Therefore, our refinement criterion is based on $1/\alpha(E)$, which is the average distance between ionization events for an electron. Ignoring advection, it is an estimate for the distance over which the electron density increases by a factor of $e \approx 2.72$. For the simulations presented here, the following criterion was used

$$\Delta x < c_0 c_1 / \alpha(c_1 E), \quad (9)$$

with $c_0 = 1$ and $c_1 = 1.2$. The constant c_1 was introduced to balance the refinement ahead and on the sides of the streamer. Without this constant (or when it is one), we sometimes observed oscillations in a streamer's radius. Setting $c_1 > 1$ increases the refinement for intermediate electric fields, as illustrated in figure 5. This helps to have more refinement on the sides of streamers, without significantly increasing the refinement at their tips. A benefit of an electric-field dependent criterion is that the electric field profile is generally smoother than that of e.g. the electron density or the space charge density. A smoother refinement criterion can help to reduce the number of refinement boundaries, at which the accuracy of the numerical schemes drops.

The criterion of equation (9) is evaluated for each grid cell. If at least one cell of a grid block requires refinement, the whole block is refined. A *five* implements a refinement buffer, so that blocks are also refined when nearby cells in neighboring blocks require refinement. For the simulations presented here, we used a buffer distance of three cells. Furthermore, the code places refinement around the initial conditions, to ensure they are accurately captured.

Grid blocks can be derefined when for all cells equation (9) holds for a small value of c_0 and when $\Delta x < \Delta x_{\text{deref}}$. Here, we have used $c_0 = 1/8$ and $\Delta x_{\text{deref}} = 30 \mu\text{m}$, where Δx_{deref} controls the mesh resolution of the discharge in regions where it no longer grows. An example of the resulting mesh around a streamer head is shown in figure 2. This streamer was generated in nitrogen at 1 bar, using the same transport coefficients as for the examples presented in section 3.

The above criterion is an empirical criterion for positive streamers, which often works quite well, but not always. For example, when simulating negative streamers propagating into a zero-density region ($n_e = 0$), the criterion will trigger refinement where there are no electrons and no space charge. We have experimented with a different criterion, based on the space charge density ρ : $\Delta x < \sqrt{c_3 \epsilon_0 / |\rho|}$, with c_3 for example 25 V. Such a criterion captures the space charge layers quite well, but not the strong density gradients ahead of those charge layers, which play an important role in streamer propagation. In the future, we hope to find a more generic criterion, based on the discretization error in the model itself.

We would like to point out that the coarse mesh can make a significant difference in the computational cost of simulations. For example, if the finest mesh spacing required in a simulation is $2 \mu\text{m}$, and the computational domain measures $(10 \text{ mm})^3$, then the actual finest mesh will have a spacing of about $1.22 \mu\text{m} = 10/2^{13} \text{ mm}$. By using a larger or smaller computational domain, the fine-grid spacing can be made to agree better with its desired value. This would allow for larger time steps, often using a smaller total number of grid cells.

2.6. Interpolation and restriction

When grid blocks are refined, the electron and ion density are interpolated to the fine-grid blocks. We currently use standard bilinear and trilinear interpolation, which has the drawback that it is non-conservative near the boundary of the refined block. In the future we will consider a conservative approach with slope limiters, as in [53]. The idea is to determine the (limited) density gradient in a coarse grid cell, and then use this slope to fill fine grid values.

When grid blocks are coarsened, the electron and ion density of the fine grid cells are averaged to obtain coarse values. For the case shown in figure 4, the coarse density $U_{3,1}$ would for example be given by $U_{3,1} = (u_{5,1} + u_{5,2} + u_{6,1} + u_{6,2})/4$, which is conservative.

2.7. Inclusion of electrodes and dielectrics

When developing a numerical code, there is often a trade-off between flexibility and computational efficiency. In the development of Afivo-streamer our focus has been on efficiency, to enable computationally costly 3D simulations. We therefore make use of a structured quadtree/octree grid, in which the inclusion of curved electrodes or curved dielectrics is not (yet) supported. It is however possible to include flat dielectrics that are aligned with the mesh, which are for example relevant for the simulation of discharges near liquids.

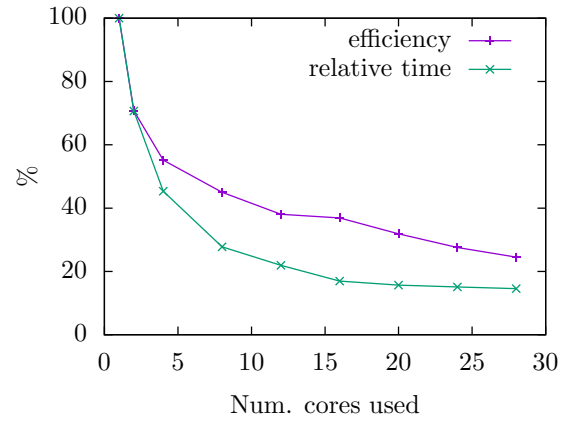


Figure 6. Parallel efficiency and relative simulation time versus the number of cores used, relative to a single core computation. The results were obtained for nodes with 28 Intel Xeon E5-2680 cores, on which we simulated case 1 of section 3.2 (a seed evolving in a homogeneous background density) up to 2.5 ns.

Support for curved geometries in Afivo-streamer could be implemented in different ways. It would for example be possible to modify the finite volume discretization to support body-fitted meshes, but this leads to problems with sharp features and the coordinate transformation can be complex in 3D. Alternatively, a cut-cell approach [54] could be implemented. Our strategy will be to first support curved geometries in the field solver, as was for example already done in [55]. Later, we will focus on the adaptation of the fluid model. It can for example be important to avoid the appearance of tiny grid cells near an object, because they would reduce the allowed time step.

3. 3D simulations

We now demonstrate the functionality of Afivo-streamer with three examples, all in 3D. The simulations were performed on a single node containing two Xeon E5-2680v4 processors (2×14 cores, at 2.4 GHz). The simulations ran for up to 24 hours, using up to 10^8 grid cells. Figure 6 illustrates the parallel scaling of the code. Individual output files with the 3D data were up to 5 gigabytes in size.

3.1. Simulation conditions

The simulations presented here were performed in nitrogen at one bar and 300 Kelvin. Electron transport coefficients (e.g. α , μ_e) were computed with Bolsig+ [43] from Phelps' cross sections [56]. A computational domain of $(40 \text{ mm})^3$ was used, constructed from octree blocks of 8^3 cells. The maximum grid spacing was set to $625 \mu\text{m}$; the minimum grid spacing in the simulations was about $2.4 \mu\text{m}$. A background electric field of $E_0 = 2.0 \text{ MV m}^{-1}$ was applied in the $-\hat{z}$ direction, which is below the 'breakdown' threshold for nitrogen. For a discussion of the difference between discharges in overvolted and undervolted conditions we refer to [57]. The background field is imposed by grounding the bottom boundary of the domain and applying 80 kV at the top. On the other sides of the

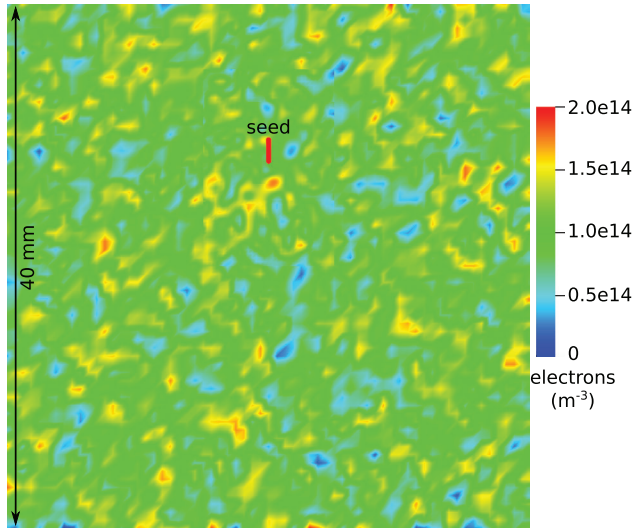


Figure 7. Cross section through the 3D computational domain for case 3, showing a stochastic background density $2U \times 10^{14} \text{ m}^{-3}$ with a correlation length of $625 \mu\text{m}$, where U is a uniform random number between zero and one. The location of the ionized seed from which the discharge starts is also visible, its density (10^{20} m^{-3}) exceeds the color scheme.

domain, Neumann zero boundary conditions were used for the potential. Neumann zero boundary conditions were also used for the electron density on all sides, but this had little effect on the results because the simulated streamers did not connect to boundaries.

The propagation of positive streamers requires free electrons ahead of them. In air, such electrons are often provided by photoionization. Since we here perform simulations in nitrogen, where photoionization is absent, a background density of 10^{14} m^{-3} electrons and positive ions is included instead. Such a density could for example be present due to previous discharges in a repetitively pulsed system [58].

To start a discharge, the background field has to be locally enhanced. We do this by placing an ionized seed of about 1.8 mm long with a radius of about 0.15 mm. The electron and positive ion density are 10^{20} m^{-3} at the center, and they decay at distances above $d = 0.1 \text{ mm}$ with a so-called *smoothstep* profile: $1 - 3x^2 + 2x^3$ up to $x = 1$, where $x = (d - 0.1 \text{ mm})/0.1 \text{ mm}$. When the electrons from a seed drift upwards, the electric field at the bottom of the seed is enhanced so that a positive streamer can form.

3.2. Stochastic background density

In this example, we investigate how a stochastic distribution of background ionization affects streamer propagation. A single ionized seed is placed as shown in figure 7. We then let a discharge evolve using three different background ionization distributions, for which the electron and positive ion density per cell are given by:

- Case 1: A constant value of 10^{14} m^{-3}
- Case 2: A stochastic value $(0.5 + U) \times 10^{14} \text{ m}^{-3}$, where U is a uniformly distributed random number between zero and one.

- Case 3: A stochastic density $2U \times 10^{14} \text{ m}^{-3}$, using the same random numbers as for case 2.

The background is created at the grid level with spacing $625 \mu\text{m}$ and then linearly interpolated to finer grids, so that the noise has a correlation length of $625 \mu\text{m}$. Note that all three cases have the same average density of 10^{14} m^{-3} . An example of the third case is shown in figure 7. We remark that the above distributions do not contain physically realistic fluctuations, in which case the number of electrons per cell would be Poisson-distributed.

Figure 8 shows how a positive streamer propagates for the different cases. Remarkably, the streamer velocity is nearly identical. This is consistent with previous studies [29, 59, 60], in which it was found that the streamer velocity only weakly depends on the background ionization level. The background density has a stronger effect on the morphology of the streamer. After 23 ns, case 3 shows streamer branching, while case 1 and 2 do not. The evolution of cases 2 and 3 seems closer to the experimentally observed streamers of figure 1. Our results agree with a previous study [61], in which it was found that positive streamer branching is accelerated by stochastic electron density fluctuations.

3.3. Interaction with preionization

This example is related to two previous studies [36, 62], in which the guiding of positive streamers by preionization from a laser was investigated. Here, we simulate a positive streamer passing through three preionized cylinders. The cylinders are aligned perpendicular to the direction of propagation, as indicated on the left of figure 9. They contain a density of 10^{16} , 10^{17} and 10^{18} m^{-3} electrons and positive ions. A background density of 10^{14} m^{-3} was present in the whole domain.

Figure 9 shows how the electron density and electric field evolve in time, and figure 10 shows the final state rotated around the vertical z -axis. Since the fluid model employed here is deterministic, the mirror symmetry in x and y of the initial conditions is preserved. Upon reaching the first preionized region, the streamer's maximum electric field is reduced, and it becomes slightly wider. Figure 10 shows that the streamer actually branches, and that the branches grow around the ionized patch. A similar effect was observed in [63], in which positive streamers grew around the preionization generated by a negative discharge.

The second patch has a similar effect to the first one. Inside the third patch, the electron density of the discharge is significantly lower. Due to the high preionization density (10^{18} m^{-3}) in this region, the streamer loses most of its electric field enhancement. A similar phenomenon was observed for sprite discharges, to explain the formation of so-called 'beads' [64]. At around 25 ns the streamer continues, and it branches at the boundary of the 10^{17} m^{-3} and 10^{18} m^{-3} preionized regions, see figure 10. As the positive streamers grows downwards, electrons drift out towards the top. These electrons could eventually form a negative streamer, as can be seen in the electric field profiles at later times.

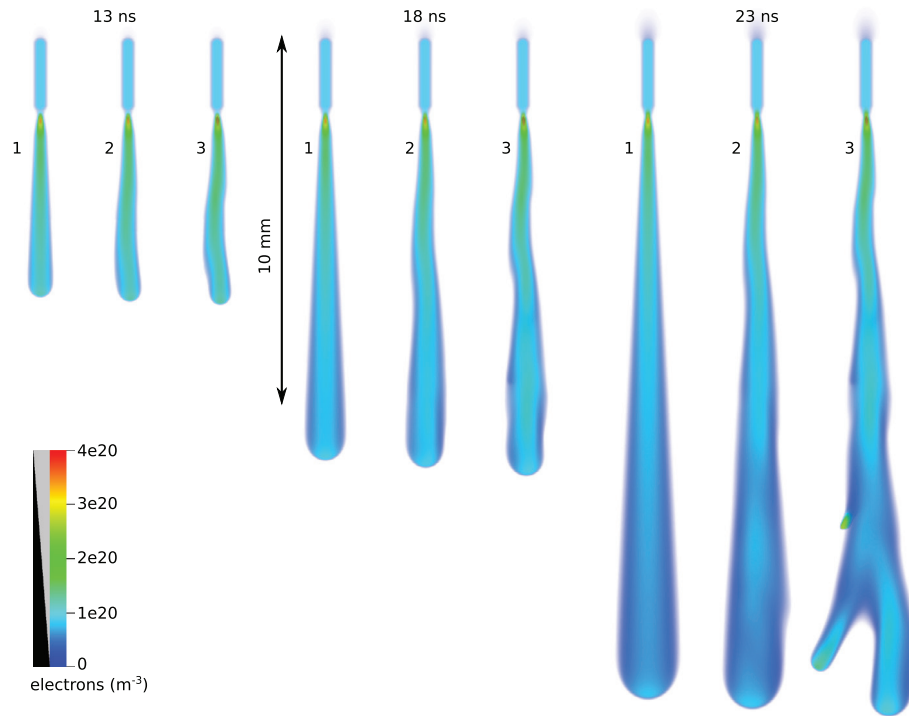


Figure 8. Evolution of a positive streamer in a 3D simulation, performed in N_2 at 1 bar with a background electric field of 2 MV/m. Three background densities are considered 1: uniform, 2: half-stochastic, 3: fully stochastic, see text. The average background density is $n_e = n_i = 10^{14} \text{ m}^{-3}$ for each case. Shown is a 3D volume rendering of the electron density; the opacity is indicated in the legend.

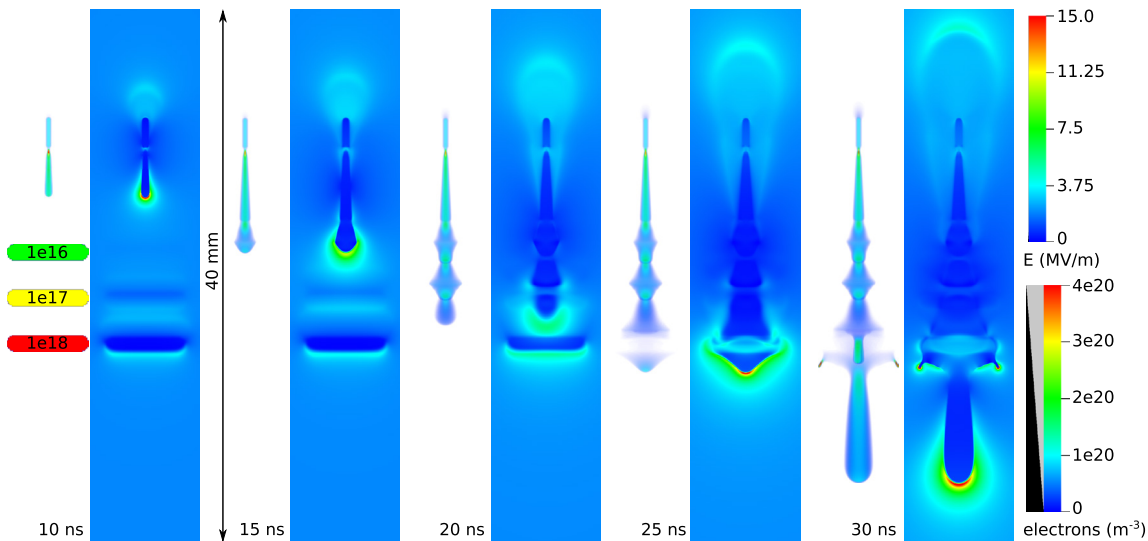


Figure 9. Evolution of a positive streamer in a 3D simulation as it propagates through preionized regions with 10^{16} , 10^{17} and 10^{18} m^{-3} electrons and positive ions. At each indicated time a 3D volume rendering of the electron density together with a cross section of the electric field is shown.

3.4. Interacting streamers

In this example, the interaction between two streamers is investigated; previous numerical and experimental investigations can be found in [25, 65]. The two interacting streamers are created by placing two field-enhancing seeds in the domain, instead of the single one used in the previous examples. We consider two cases, in which the vertical offset between the seeds is 4 mm or 8 mm; their horizontal offset is 4 mm.

Figure 11 shows the time evolution of the electron density and the electric field for both cases, with equipotential lines indicated at steps of 4 kV. With the smaller vertical offset, the streamers repel, whereas they attract with the larger offset. This can be explained by looking at the equipotential lines. For the case with the smaller vertical offset, the lower streamer bends equipotential lines downwards. This reduces the electric field in which the upper streamer propagates. The

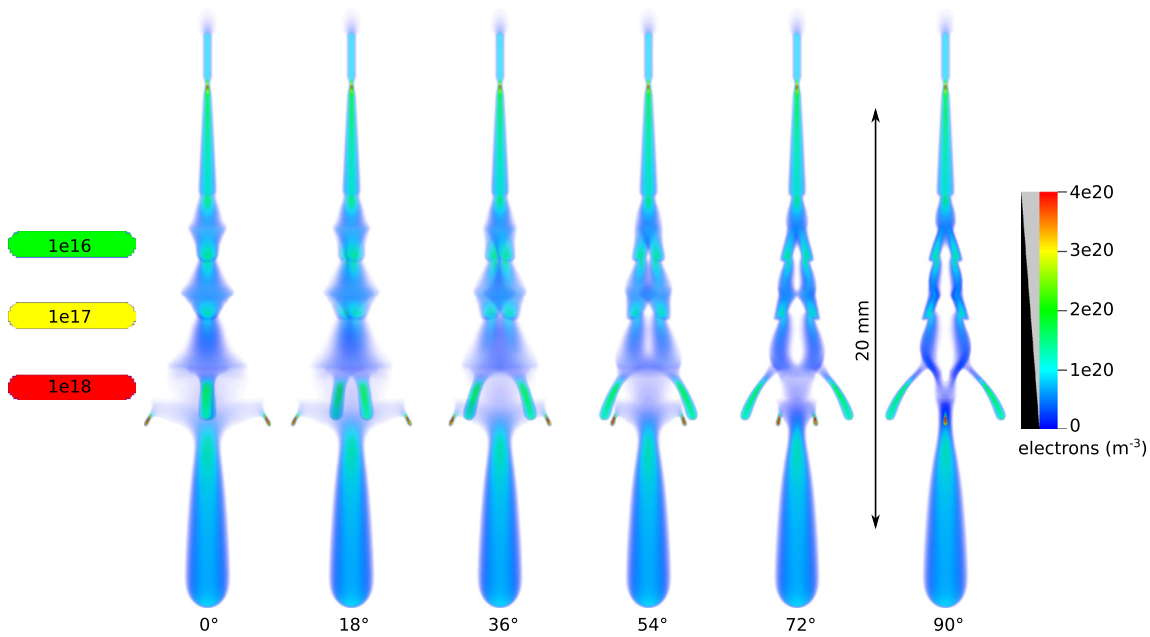


Figure 10. Rotated views of the electron density at 30 ns for a positive streamer that has propagated through preionized patches, as in the last stage of figure 9. The views are rotated around the vertical z -axis, in steps of 18° . Note how the streamer branches and grows around the preionized regions while preserving mirror symmetry in x and y .

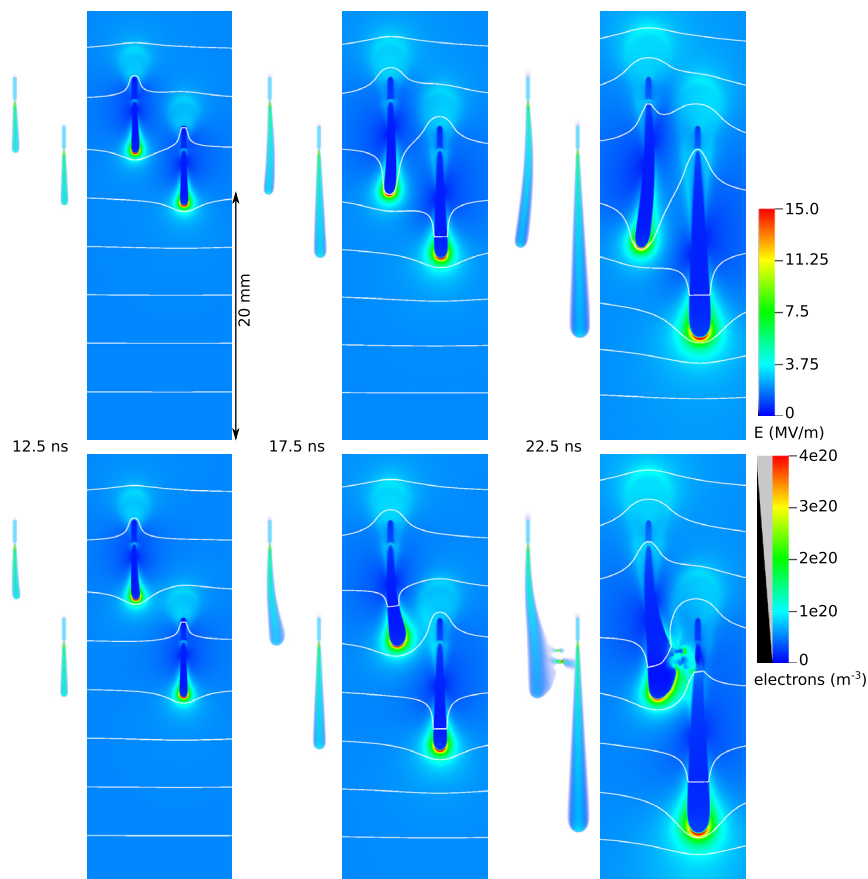


Figure 11. Evolution of two interacting positive streamers in 3D. The streamers have a vertical offset of 4 mm (top row) or 8 mm (bottom row) and a horizontal offset of 4 mm. At each indicated time, a 3D volume rendering of the electron density together with a cross section of the electric field are shown. The white equipotential lines are spaced by 4 kV.

reduction is smaller farther away from the lower streamer, which causes the upper streamer to bend outwards.

For the case with the larger vertical offset, another effect becomes important. Both streamers are *in total* electrically neutral (as well as the seeds they originate from). Their bottom/positive end therefore bends equipotential lines downwards, whereas their upper/negative end bends them upwards. With sufficient vertical offset between the streamers, the equipotential lines between them are therefore compressed. This means there is an increased electric field between them, so that they attract. In summary, positively charged streamer heads repel, whereas a positive streamer head is attracted to a negatively charged streamer tail. Finally, notice how in both cases the bottom streamer propagates almost straight down, whereas path of the upper streamer is bent.

4. Conclusions and outlook

We have presented Afivo-streamer, an open-source plasma fluid model for 2D, cylindrical and 3D simulations of streamer discharges. The model makes use of the Afivo framework [35] to provide adaptive mesh refinement, a geometric multigrid Poisson solver and OpenMP parallelization. For robustness, the fluid model is of the drift-diffusion-reaction type in combination with the local field approximation. We have described the numerical implementation of Afivo-streamer, discussing also the refinement criterion. The model's capabilities have been demonstrated with 3D examples of positive streamers in under-volted gaps in pre-ionized nitrogen at 1 bar. In the first example the effect of stochastic background ionization on streamer propagation and branching was investigated. The second example demonstrated how a streamer interacts with preionized patches, in which it slows down and loses much of its field enhancement. Streamer branching was also observed. The third example investigated how streamers can attract or repel, depending on their relative position. These simulations used up to 10^8 grid cells, and all ran within a day. A uniform grid with the same resolution would have required $4 \cdot 10^{12}$ grid cells.

Future work will focus on the effects of photoionization, which was not included here, but is important for discharges in air. Support for the inclusion of curved electrodes or dielectrics, which are relevant for many physical applications, is planned for a future version of Afivo-streamer.

Acknowledgments

JT acknowledges support by postdoctoral fellowship 12Q6117N from Research Foundation—Flanders (FWO) and earlier support from STW project 10755.

ORCID iDs

Jannis Teunissen  <https://orcid.org/0000-0003-0811-5091>
Ute Ebert  <https://orcid.org/0000-0003-3891-6869>

References

- [1] Vitello P A, Penetrante B M and Bardsley J N 1994 Simulation of negative-streamer dynamics in nitrogen *Phys. Rev. E* **49** 5574–98
- [2] Yi W J and Williams P F 2002 Experimental study of streamers in pure N_2 and N_2/O_2 mixtures and a ≈ 13 cm gap *J. Phys. D: Appl. Phys.* **35** 205–18
- [3] Ebert U, Nijdam S, Li C, Luque A, Briels T and van Veldhuizen E 2010 Review of recent results on streamer discharges and discussion of their relevance for sprites and lightning *J. Geophys. Res.* **115** A00E43
- [4] Sentman D D and Wescott E M 1995 Red sprites and blue jets: thunderstorm-excited optical emissions in the stratosphere, mesosphere, and ionosphere *Phys. Plasmas* **2** 2514
- [5] Černák M, Kováčik D, Ráhel J, Stahel P, Zahoranová A, Kubincová J, Tóth A and Černáková L 2011 Generation of a high-density highly non-equilibrium air plasma for high-speed large-area flat surface processing *Plasma Phys. Control. Fusion* **53** 124031
- [6] Akiyama H 2000 Streamer discharges in liquids and their applications *IEEE Trans. Dielectr. Electr. Insul.* **7** 646–53
- [7] Nastuta A V, Topala I, Grigoras C, Pohoata V and Popa G 2011 Stimulation of wound healing by helium atmospheric pressure plasma treatment *J. Phys. D: Appl. Phys.* **44** 105204
- [8] Sands B L, Ganguly B N and Tachibana K 2008 A streamer-like atmospheric pressure plasma jet *Appl. Phys. Lett.* **92** 151503
- [9] Briels T M P, van Veldhuizen E M and Ebert U 2008 Positive streamers in air and nitrogen of varying density: experiments on similarity laws *J. Phys. D: Appl. Phys.* **41** 234008
- [10] Dhali S and Williams P 1985 Numerical simulation of streamer propagation in nitrogen at atmospheric pressure *Phys. Rev. A* **31** 1219–21
- [11] Bourdon A, Pasko V P, Liu N Y, Célestin S, Ségur P and Marode E 2007 Efficient models for photoionization produced by non-thermal gas discharges in air based on radiative transfer and the helmholtz equations *Plasma Sources Sci. Technol.* **16** 656–78
- [12] Kulikovskiy A A 1995 A more accurate Scharfetter–Gummel algorithm of electron transport for semiconductor and gas discharge simulation *J. Comput. Phys.* **119** 149–55
- [13] Liu N 2004 Effects of photoionization on propagation and branching of positive and negative streamers in sprites *J. Geophys. Res.* **109** A04301
- [14] Morrow R and Lowke J J 1997 Streamer propagation in air *J. Phys. D: Appl. Phys.* **30** 614–27
- [15] Georghiou G E, Morrow R and Metaxas A C 2000 A two-dimensional, finite-element, flux-corrected transport algorithm for the solution of gas discharge problems *J. Phys. D: Appl. Phys.* **33** 2453–66
- [16] Montijn C, Hundsdorfer W and Ebert U 2006 An adaptive grid refinement strategy for the simulation of negative streamers *J. Comput. Phys.* **219** 801–35
- [17] Eichwald O, Bensaad H, Ducasse O and Yousfi M 2012 Effects of numerical and physical anisotropic diffusion on branching phenomena of negative-streamer dynamics *J. Phys. D: Appl. Phys.* **45** 385203
- [18] Bessières D, Paillol J, Bourdon A, Ségur P and Marode E 2007 A new one-dimensional moving mesh method applied to the simulation of streamer discharges *J. Phys. D: Appl. Phys.* **40** 6559–70
- [19] Zhuang C, Zeng R, Zhang B and He J 2014 A WENO scheme for simulating streamer discharge with photoionizations *IEEE Trans. Magn.* **50** 325–8

- [20] Georghiou G, Morrow R and Metaxas A 1999 An improved finite-element flux-corrected transport algorithm *J. Comput. Phys.* **148** 605–20
- [21] Ducasse O, Papageorghiou L, Eichwald O, Spyrou N and Yousfi M 2007 Critical analysis on two-dimensional point-to-plane streamer simulations using the finite element and finite volume methods *IEEE Trans. Plasma Sci.* **35** 1287–300
- [22] OSullivan F, Hwang J, Zahn M, Hjortstam O, Pettersson L, Liu R and Biller P 2008 A model for the initiation and propagation of positive streamers in transformer oil *Conf. Record of the 2008 IEEE Int. Symp. on Electrical Insulation* (<https://doi.org/10.1109/ELINSL.2008.4570312>)
- [23] Kulikovskiy A 1998 Three-dimensional simulation of a positive streamer in air near curved anode *Phys. Lett. A* **245** 445–52
- [24] Pancheshnyi S, Ségur P, Capellière J and Bourdon A 2008 Numerical simulation of filamentary discharges with parallel adaptive mesh refinement *J. Comput. Phys.* **227** 6574–90
- [25] Luque A, Ebert U and Hundsdorfer W 2008 Interaction of streamer discharges in air and other oxygen–nitrogen mixtures *Phys. Rev. Lett.* **101** 075005
- [26] Chanrion O and Neubert T 2008 A PIC-MCC code for simulation of streamer propagation in air *J. Comput. Phys.* **227** 7222–45
- [27] Rose D V, Welch D R, Clark R E, Thoma C, Zimmerman W R, Bruner N, Rambo P K and Atherton B W 2011 Towards a fully kinetic 3D electromagnetic particle-in-cell model of streamer formation and dynamics in high-pressure electronegative gases *Phys. Plasmas* **18** 093501
- [28] Li C, Ebert U and Hundsdorfer W 2012 Spatially hybrid computations for streamer discharges: II. Fully 3D simulations *J. Comput. Phys.* **231** 1020–50
- [29] Teunissen J and Ebert U 2016 3D PIC-MCC simulations of discharge inception around a sharp anode in nitrogen/oxygen mixtures *Plasma Sources Sci. Technol.* **25** 044005
- [30] Kolobov V and Arslanbekov R 2016 Electrostatic PIC with adaptive cartesian mesh *J. Phys.: Conf. Ser.* **719** 012020
- [31] Papageorgiou L, Metaxas A C and Georghiou G E 2011 Three-dimensional numerical modelling of gas discharges at atmospheric pressure incorporating photoionization phenomena *J. Phys. D: Appl. Phys.* **44** 045203
- [32] Lavesson N, Jogenfors J and Widlund O 2014 Modeling of streamers in transformer oil using openfoam *COMPEL Int. J. Comput. Math. Electr. Electron. Eng.* **33** 1272–81
- [33] Kolobov V and Arslanbekov R 2012 Towards adaptive kinetic-fluid simulations of weakly ionized plasmas *J. Comput. Phys.* **231** 839–69
- [34] Popinet S 2003 Gerris: a tree-based adaptive solver for the incompressible euler equations in complex geometries *J. Comput. Phys.* **190** 572–600
- [35] Teunissen J and Ebert U 2017 Afivo: a framework for quadtree/octree amr with shared-memory parallelization and geometric multigrid methods *Comput. Phys. Commun.* (arXiv:1701.04329)
- [36] Nijdam S, Teunissen J, Takahashi E and Ebert U 2016 The role of free electrons in the guiding of positive streamers *Plasma Sources Sci. Technol.* **25** 044001
- [37] CWI Multiscale Dynamics group webpage <http://cwimd.nl>
- [38] Brandt A and Livne O E 2011 *Multigrid Techniques* (Philadelphia: SIAM)
- [39] Trottenberg U, Oosterlee C and Schuller A 2000 *Multigrid* (Amsterdam: Elsevier)
- [40] Briggs W L, Henson V E and McCormick S F 2000 *A Multigrid Tutorial* 2nd edn (Philadelphia: SIAM)
- [41] Childs H *et al* 2012 *VisIt: An End-User Tool For Visualizing, Analyzing Very Large Data (High Performance Visualization—Enabling Extreme-Scale Scientific Insight)* (London: Chapman and Hall) pp 357–72
- [42] Luque A and Ebert U 2012 Density models for streamer discharges: beyond cylindrical symmetry and homogeneous media *J. Comput. Phys.* **231** 904–18
- [43] Hagelaar G J M and Pitchford L C 2005 Solving the Boltzmann equation to obtain electron transport coefficients and rate coefficients for fluid models *Plasma Sources Sci. Technol.* **14** 722–33
- [44] Dujko S, Ebert U, White R D and Petrović Z L 2011 Boltzmann equation analysis of electron transport in a N₂-O₂ streamer discharge *Japan. J. Appl. Phys.* **50** 08JC01
- [45] Li C, Ebert U and Hundsdorfer W 2010 Spatially hybrid computations for streamer discharges with generic features of pulled fronts: I. Planar fronts *J. Comput. Phys.* **229** 200–20
- [46] Markosyan A H, Teunissen J, Dujko S and Ebert U 2015 Comparing plasma fluid models of different order for 1d streamer ionization fronts *Plasma Sources Sci. Technol.* **24** 065002
- [47] Becker M M, Khlert H, Sun A, Bonitz M and Loffhagen D 2017 Advanced fluid modeling and PIC/MCC simulations of low-pressure ccrf discharges *Plasma Sources Sci. Technol.* **26** 044001
- [48] Eichwald O, Ducasse O, Merbahi N, Yousfi M and Dubois D 2005 Effect of order fluid models on flue gas streamer dynamics *J. Phys. D: Appl. Phys.* **39** 99107
- [49] Pancheshnyi S 2014 Photoionization produced by low-current discharges in O₂, air, N₂ and CO₂ *Plasma Sources Sci. Technol.* **24** 015023
- [50] Teunissen J 2015 3D simulations and analysis of pulsed discharges *PhD Thesis Technische Universiteit Eindhoven* <http://repository.tue.nl/801516>
- [51] Koren B 1993 A robust upwind discretization method for advection, diffusion, source terms *Numerical Methods for Advection-Diffusion Problems* ed C Vreugdenhil and B Koren (Braunschweig/Wiesbaden: Vieweg) pp 117–38
- [52] Hundsdorfer W and Verwer J G 2003 *Numerical Solution of Time-Dependent Advection-Diffusion-Reaction Equations (Springer Series in Computational Mathematics vol 33)* 1st edn (Berlin: Springer)
- [53] Keppens R, Meliani Z, van Marle A, Delmont P, Vlasis A and vander Holst B 2012 Parallel, grid-adaptive approaches for relativistic hydro and magnetohydrodynamics *J. Comput. Phys.* **231** 718–44
- [54] Hartmann D, Meinke M and Schröder W 2011 A strictly conservative cartesian cut-cell method for compressible viscous flows on adaptive grids *Comput. Methods Appl. Mech. Eng.* **200** 1038–52
- [55] Celestin S, Bonaventura Z, Zeghondy B, Bourdon A and Ségur P 2009 The use of the ghost fluid method for Poisson's equation to simulate streamer propagation in point-to-plane and point-to-point geometries *J. Phys. D: Appl. Phys.* **42** 065203
- [56] Phelps A V and Pitchford L C 1985 Anisotropic scattering of electrons by N₂ and its effect on electron transport *Phys. Rev. A* **31** 2932–49
- [57] Sun A, Teunissen J and Ebert U 2014 The inception of pulsed discharges in air: simulations in background fields above and below breakdown *J. Phys. D: Appl. Phys.* **47** 445205
- [58] Nijdam S, Takahashi E, Markosyan A and Ebert U 2014 Investigation of positive streamers by double pulse experiments, effects of repetition rate and gas mixture *Plasma Sources Sci. Technol.* **23** 025008
- [59] Nijdam S, Wormeester G, van Veldhuizen E M and Ebert U 2011 Probing background ionization: positive streamers with varying pulse repetition rate and with a radioactive admixture *J. Phys. D: Appl. Phys.* **44** 455201

- [60] Wormeester G, Pancheshnyi S, Luque A, Nijdam S and Ebert U 2010 Probing photo-ionization: simulations of positive streamers in varying N₂:O₂-mixtures *J. Phys. D: Appl. Phys.* **43** 505201
- [61] Luque A and Ebert U 2011 Electron density fluctuations accelerate the branching of positive streamer discharges in air *Phys. Rev. E* **84** 046411
- [62] Nijdam S, Takahashi E, Teunissen J and Ebert U 2014 Streamer discharges can move perpendicularly to the electric field *New J. Phys.* **16** 103038
- [63] Nijdam S, Miermans K, van Veldhuizen E M and Ebert U 2011 A peculiar streamer morphology created by a complex voltage pulse *IEEE Trans. Plasma Sci.* **39** 2216–7
- [64] Luque A and Gordillo-Vzquez F J 2011 Sprite beads originating from inhomogeneities in the mesospheric electron density *Geophys. Res. Lett.* **38** L04808
- [65] Nijdam S, Geurts C G C, van Veldhuizen E M and Ebert U 2009 Reconnection and merging of positive streamers in air *J. Phys. D: Appl. Phys.* **42** 045201